# High Performance Gas Diffusion Layer with Hydrophobic Nanolayer under a Supersaturated Operation Condition for Fuel Cells

Tae-Jun Ko,[†,‡] Sae Hoon Kim,[§] Bo Ki Hong,*[,§] Kwang-Ryeol Lee,[†] Kyu Hwan Oh,[‡] and Myoung-Woon Moon*[,†]

[†]Institute for Multidisciplinary Convergence of Matter, Korea Institute of Science and Technology, Seoul 136-791, Republic of Korea
[‡]Department of Materials Science and Engineering, Seoul National University, Seoul 151-742, Republic of Korea
[§]Fuel Cell Vehicle Team 1, Eco-Technology Center, Hyundai-Kia Motors, Yongin-Si, Gyeonggi-Do 446-912, Republic of Korea

**ABSTRACT:** Reliable operation of a proton exchange membrane fuel cell requires proper water management to prevent water flooding in porous carbon materials such as the gas diffusion layer (GDL). In contrast to the conventional GDL that uses the "wet" dip-coating process with solvent and expensive polytetrafluoroethylene, we have proposed a novel GDL with a controlled hydrophobic silicone (i.e., hexamethyldisiloxane) nanolayer by a highly efficient and cost-effective "dry" deposition process. The GDL with the nanolayer exhibited an increased contact angle, decreased contact angle hysteresis, and suppressed water condensation. Even though the GDL with the nanolayer had a higher electrical resistance than the pristine GDL, the cell performance of the GDL with an optimum nanolayer thickness of 8.6 nm was practically the same as that of the pristine GDL under normal operating conditions. Under a supersaturated condition, the GDL with optimum nanolayer thickness exhibited much higher cell performance than the pristine GDL over all current densities due to enhanced hydrophobicity. Long-term operational stability and dynamic response of the GDL with the nanolayer were much improved over those of the pristine GDL.

**KEYWORDS:** gas diffusion layer, flooding, water condensation, hydrophobic coating, supersaturation
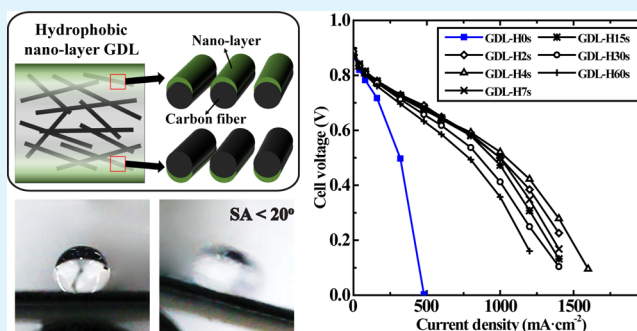


## 1. INTRODUCTION

The importance of developing renewable energy has increased due to the depletion of fossil fuels and the recognition of environmental problems. Proton exchange membrane fuel cells (PEMFCs) in particular are one of the prospective renewable energy sources for alternative clean and green energy in the automobile industry because of their several advantages, including high efficiency, low operation temperature, and zero gas emissions exhaust.[1−5] However, to commercialize PEMFCs, crucial issues such as the high cost of materials and some technical barriers need to be solved. Among the technical issues, water flooding in porous carbon materials (i.e., the gas diffusion layer (GDL)) is a critical problem that decreases cell performance.[4,6−8] Under high current density or in severe operating conditions such as low temperature and/or high humidity, water management issues in PEMFCs are particularly critical.[9−11] For instance, a fuel cell vehicle (FCV) may experience a transient supersaturation condition during an operational process from a cold start-up at low temperatures (i.e., ambient or subfreezing conditions) to typical cell operation at high temperatures (i.e., 60−80 °C), especially when relatively warm and humid reactant gases may be fed to a cool cell, causing significant liquid water flooding and condensation in the fuel cell.[12,13] For an FCV to operate

stably under a variety of operating conditions, the PEMFC needs to perform normally under several transient supersaturation conditions as well. When product water formed from the oxygen reduction reaction at the cathode is not discharged properly out of the cells, redundant water blocks the pores in porous carbon materials, resulting in water flooding and cell performance decay. This water flooding problem prevents reactant gases from being transported to the membrane−electrode assembly (MEA) of a fuel cell and causes a drastic loss in cell voltage.[14] To hinder or minimize water flooding, many studies have been conducted in an attempt to increase hydrophobicity or water repellency of porous carbon materials like the GDL. In PEMFCs, the GDL plays an important role in transporting reactant gases, conducting electrons from electrodes to the bipolar plate, and eliminating product water out of the fuel cell. The GDL typically consists of a microporous layer (MPL) and a macroporous substrate or backing. The MPL is generally composed of a hydrophobic agent and carbon black powder, whereas the macroporous substrate consists of a hydrophobic agent and carbon fibers based on felt, paper, or

cloth structures.[15−17] There are two main advantages when hydrophobicity is promoted in the GDL. First, the amount of condensed water is reduced by suppressing the water condensation rate. Second, condensed water drops can easily be removed from the GDL due to low adhesion between the water droplet and the GDL. In the case of commercial GDL products for FCV applications, fluorinated polymers (i.e., polytetrafluoroethylene (PTFE), fluorinated ethylene propylene, etc.) are most commonly used as the hydrophobic agent for GDLs using a "wet" dip-coating process.[16−19] However, the conventional dip-coating process normally uses an aqueous PTFE suspension and thus the remaining solvent needs to be removed by drying for at least several hours, followed by an additional sintering process at high temperature (i.e., up to 350 °C) to fix the PTFE to the GDL. In addition, the PTFE distribution in GDLs is known to be highly sensitive to the solvent drying process, which makes it difficult to guarantee a uniform quality of conventional GDLs.[13,17] Rofaiel et al. reported that the through-plane distributions of PTFE in commercial GDLs based on carbon fiber felt and paper were neither uniform nor homogeneous, and the PTFE appeared to have a bimodal distribution.[20]

Additionally, it is well-known that fluorinated polymers have several issues regarding high production costs mainly due to the unusual polymerization process, health concerns, and the large amount of expensive materials required for the GDLs (i.e., 5−30 wt %).[21−23] Because of these drawbacks of fluorinated materials, Wang et al. recently tried to use nonfluorinated materials, that is, a mixture of silica particles and polydimethylsiloxane, as a hydrophobic agent for GDL, but this method still employed a conventional coating and curing process at 180 °C.[21] Thus, the conventional dip-coating process for GDLs, which typically adopts fluorinated materials is a complicated, expensive, and time-consuming process and needs to be improved to facilitate the mass production of GDLs. Moreover, the dip-coating method tends to block pores that could be used for the gas flow path, consequently causing a decrease in the cell efficiency.

It is well-known that the plasma technique is a fast, clean, and "dry" method that does not require a solvent. In addition, it does not significantly deteriorate the intrinsic bulk properties of the substrate. Recently, an alternative process employing plasma technology has been introduced to overcome disadvantages of the conventional dip-coating process.[24,25] Shiue and co-workers have reported that plasma treatment of GDLs using fluorinated materials, such as $CF_4$ and $CHF_3$, for 40 min reaction times could enhance the hydrophobicity of GDLs and ultimately fuel cell performances.[24,25] They also studied a gas diffusion electrode using a PTFE-like film with thicknesses of 200−2700 nm by a $CHF_3$ plasma technology.[26] Although several pioneering works have contributed much to the basic understanding of the hydrophobic behavior of GDLs, deep understanding and systematic studies on these phenomena under automotive operating conditions are lacking.

To develop highly hydrophobic and cost-effective GDLs for FCVs by combining nonfluorinated materials with a simple and highly efficient "dry" process, we have in this study employed a novel silicone-based material with low surface energy, hexamethyldisiloxane (HMDSO, $(CH_3)_3$-Si-O-Si-$(CH_3)_3$), and a plasma deposition process. The silicone-based material formed by plasma deposition of HMDSO vapor is known for its high corrosion resistance, low friction coefficient, and low surface energy.[27] A silicone-based hydrophobic nanolayer with a precisely controlled thickness was deposited on the GDL surface, which caused the GDL surface to become slippery and for water droplets to roll off easily. To characterize the GDL with the hydrophobic nanolayer, wettability was observed to explain the roll off behavior of macroscale water droplets, and water condensation in an environmental chamber was investigated to elucidate the condensation behavior of microscale vapor, which may be closely related to the water flooding behavior of GDL under a real operation condition of PEMFC. To examine the effect of the novel hydrophobicity process, the intrinsic characteristics of the GDL and fuel cell performances under both normal and supersaturated conditions have been investigated extensively.

## 2. MATERIAL AND METHODS

**A. Sample Preparation.** All GDL samples used in this study were composed of a carbon fiber felt-based macroporous substrate only, without an MPL to eliminate any combined effects from an MPL. A pristine GDL without any PTFE (10AA grade, SGL Technologies, GmbH, Germany) was chosen as a model GDL for plasma deposition. The average and standard deviation of thickness of the pristine GDL was approximately $373 \pm 14$ $\mu$m by 20 individual measurements (KWC 576 thickness gauge, Mitutoyo Co., Japan). A hydrophobic nanolayer was deposited on GDL surfaces via radio frequency plasma enhanced chemical vapor deposition (rfPECVD) with HMDSO (Sigma-Aldrich Co., St Louis, MO) as a precursor. A hydrophobic $SiO_x$−C:H nanolayer, with a surface energy of 24 mN/m, is deposited by plasma polymerization of the HMDSO.[28−30] At a bias voltage of $-400$ $V_b$ and a pressure of 10 mTorr, the thickness of the hydrophobic nanolayer was precisely controlled to have a specific desired value. Key characteristics of all of the GDL samples used in this study are summarized in Table 1. In this study, both surfaces of a given GDL

**Table 1. Characteristics of the GDL Samples Used in this Study**

| sample | average GDL thickness ($\mu$m) | total nanolayer deposition time (sec) | total nanolayer thickness (nm) |
|---|---|---|---|
| GDL-H0s | $373 \pm 14$ | 0 | 0 |
| GDL-H2s | $373 \pm 14$ | $2 \times 2$ | $4.3 \times 2$ |
| GDL-H4s | $373 \pm 14$ | $4 \times 2$ | $8.6 \times 2$ |
| GDL-H7s | $373 \pm 14$ | $7 \times 2$ | $16.6 \times 2$ |
| GDL-H15s | $373 \pm 14$ | $15 \times 2$ | $26.1 \times 2$ |
| GDL-H30s | $373 \pm 14$ | $30 \times 2$ | $56.1 \times 2$ |
| GDL-H60s | $373 \pm 14$ | $60 \times 2$ | $110.5 \times 2$ |

were treated by plasma polymerization of HMDSO, and the GDL sample notation was based on the HMDSO deposition time for one surface of the GDL as depicted in Figure 1a. In the case of the GDL sample denoted as GDL-H2s in Table 1 for instance, one surface of the GDL was first deposited with HMDSO for 2 s, and then the other (opposite) surface of the GDL was also deposited for 2 s, resulting in a total deposition time of 4 s.

A commercially available perfluorinated sulfonic acid MEA with a catalyst-coated membrane structure was used in this study. The MEA had an active area of $5 \times 5$ $cm^2$, and both the anode and cathode were composed of typical Pt/C catalysts. The Pt loadings of the anode and cathode were 0.1 and 0.4 mg Pt $cm^{-2}$, respectively. In-house graphite bipolar plates were used in this study. The flow field of the bipolar plate was a serpentine pattern made by a machining process. A fluorinated rubber was used as a gasket. Single fuel cells were assembled at a compression pressure of ∼0.35 MPa, which was estimated using pressure measurement films (Prescale film, FUJIFILM Corp., Japan).

**B. Surface Analysis.** To observe the surface morphology before and after hydrophobic nanolayer deposition on GDLs, a scanning electron microscope (SEM, Nova NanoSEM 200, FEI, Hillsboro, OR)
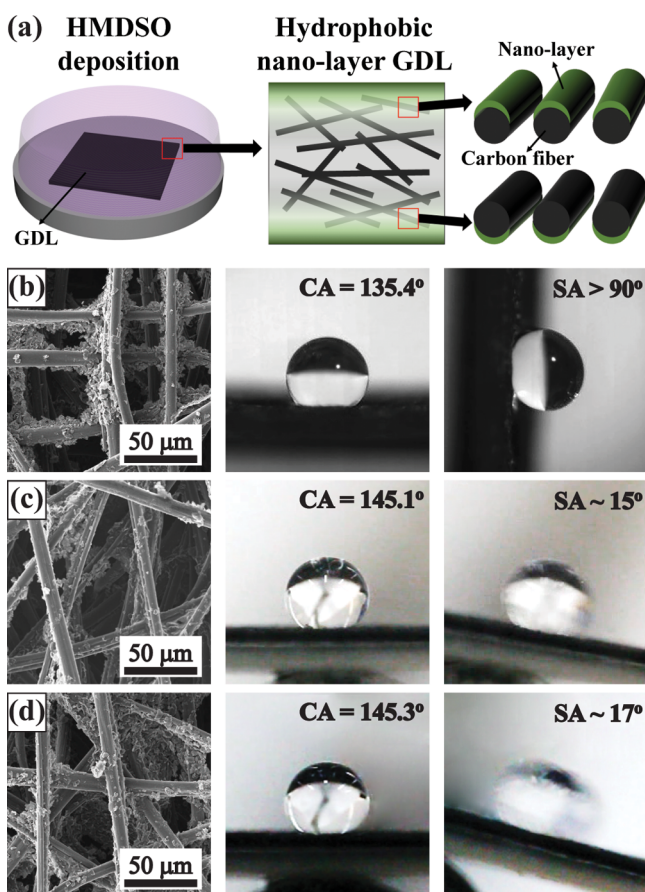
**Figure 1.** (a) Schematic of hydrophobic nanolayer GDL fabrication. A hydrophobic nanolayer was deposited on both sides of pristine GDL surfaces via the HMDSO plasma polymerization method with rfPECVD. SEM images of GDLs (left photos) and optical images of water droplets (middle and right photos) for measuring the sliding angle on the pristine and hydrophobic nanolayer GDLs with (b) pristine GDL (GDL-H0s), (c) GDL-H4s, and (d) GDL-H60s.

with a 10 kV electron acceleration voltage was employed to take micrographs of the pristine and hydrophobic nanolayer GDLs. The thickness of the hydrophobic nanolayer was measured with an atomic force microscope (AFM, XE-70, Park Systems, Korea). The bare Si wafer was used to measure the thickness of the hydrophobic nanolayer, which was simultaneously deposited on GDL samples in the same vacuum chamber.

**C. Sessile Droplet Test.** The sliding angles (SAs) of water droplets on the pristine and hydrophobic nanolayer GDLs were measured with a high-speed video camera (APX-RS, Photron, Marlow, UK) by recording images up to 1000 frames per second. Also, water wettability of the pristine and hydrophobic nanolayer GDLs was characterized by measuring the water contact angle (CA) and the contact angle hysteresis (CAH) of deionized (DI) water with a sessile drop test. For measuring CAs, ~5 $\mu$L droplets were gently deposited on the GDL surfaces using a microsyringe. The CAH was determined by calculating the difference between the advancing CA (ACA) and receding CA (RCA). The ACA was measured as DI water was added to a sessile drop, and the RCA was measured as DI water was removed from the sessile drop using a microsyringe. The CA and CAH values were measured using a goniometer (Rame-Hart, Mountain Lakes, NJ) in ambient air at 20 °C with a relative humidity (RH) of 20−35%. The CAs of each sample were measured on at least five different spots, and the average and standard deviation values are reported.

**D. Water Condensation Test.** The water condensation behavior was observed with an environmental scanning electron microscope (ESEM, XL-30 FEG, FEI, Hillsboro, OR). We explored the water condensation behavior with respect to the pressure holding duration at the supersaturation state of 5.8 Torr at 2 °C, which was maintained by a cold stage module.[29]

**E. Electrical Resistance Measurement.** Through-plane electrical resistances of GDL samples were measured as a function of compression pressure using a commercial tester (CPRT tester model, LCDV Co., Korea). A GDL specimen with an annulus type (3.0 and 1.7 cm outer and inner diameter, respectively) was placed between two highly conductive plates, and then the electrical resistance of the GDL was measured as the compression pressure was increased to 1.5 MPa. Seven individual measurements were used to estimate the average and standard deviation of the electrical resistances. A detailed description of the tester was previously described.[31]

**F. Electrochemical Cell Performance Test.** Electrochemical cell performances of PEMFCs in terms of current density−voltage (I−V) curves were measured using a single cell by a commercial tester (SMART II model, Won-A Tech Co., Korea). Both the anode (hydrogen) and cathode (air) gases were humidified to maintain a desired RH condition. The humidifier temperature ($T_{humidifier}$) was kept at 65 °C throughout all of the tests, whereas the cell temperature ($T_{cell}$) was maintained at either 65 °C for a normal condition (RH (anode/cathode) = 100%/100%) or 45 °C for a supersaturated condition. Stoichiometric ratios of hydrogen/air (1.5:2.0) were maintained to be constant for all of the tests. A single cell was fully activated at 65 °C by load cycling, and then the I−V performance of the single cell was measured up to 1600 mA cm$^{-2}$. After, the single cell was quickly cooled to 45 °C, while the humidifier temperature was maintained at 65 °C. An additional cell activation was then performed at 45 °C under supersaturated conditions followed by electrochemical I−V cell performance measurements. For a quantitative comparison of cell performances among GDL samples, the current density values of fuel cells at 0.50 V were also obtained from the I−V curves using an interpolation method. Finally, to estimate the long-term stability of the fuel cell under supersaturated conditions and the dynamic response to a transient change of the FCV speed, the cell voltages upon a rapid change of current density were monitored as a function of cell duration time at a given current density. Specifically, the current density was first maintained at 0 mA cm$^{-2}$ for 2 min, which is open circuit voltage (OCV) status, and was then increased to 320 mA cm$^{-2}$ for 10 min and finally up to 1000 mA cm$^{-2}$ for 10 min.

## 3. RESULTS AND DISCUSSION

**A. Surface Morphology and Nanolayer Thickness.** Figure 1 shows the representative surface morphology of GDLs. Also shown in Figure 1, the water droplet behavior of the hydrophobic nanolayer GDLs (GDL-H4s and -H60s) is substantially different from that of the pristine GDL (GDL-H0s). After HMDSO deposition, the CA of the water droplet increases from 135.4° to 145.1−145.3° and the SA decreases from 90° to 15−17°; thus, the GDLs became slippery surfaces allowing water droplets to easily roll off.

SEM observations were performed to compare the morphological changes of GDL surfaces with nanolayer deposition. As shown in Figure 1b, the pristine GDL (GDL-H0s) was observed to consist of carbon fibers that are 7−8 $\mu$m in diameter. Also, many macropores between the carbon fibers were observed due to a disordered network structure. In the case of the GDLs with a hydrophobic nanolayer in Figure 1c and d, there is no significant morphological change in the carbon fiber surface or pores, indicating that nanolayer deposition with PECVD may not significantly alter the pore structure due to its nanoscale coverage on the carbon fibers. The deposition rate of the hydrophobic nanolayer was measured on a flat Si wafer using an AFM. The thicknesses were measured as 4.3, 8.6, 16.6, 26.1, 56.1, and 110.5 nm at plasma deposition times of 2, 4, 7, 15, 30, and 60 s, respectively.
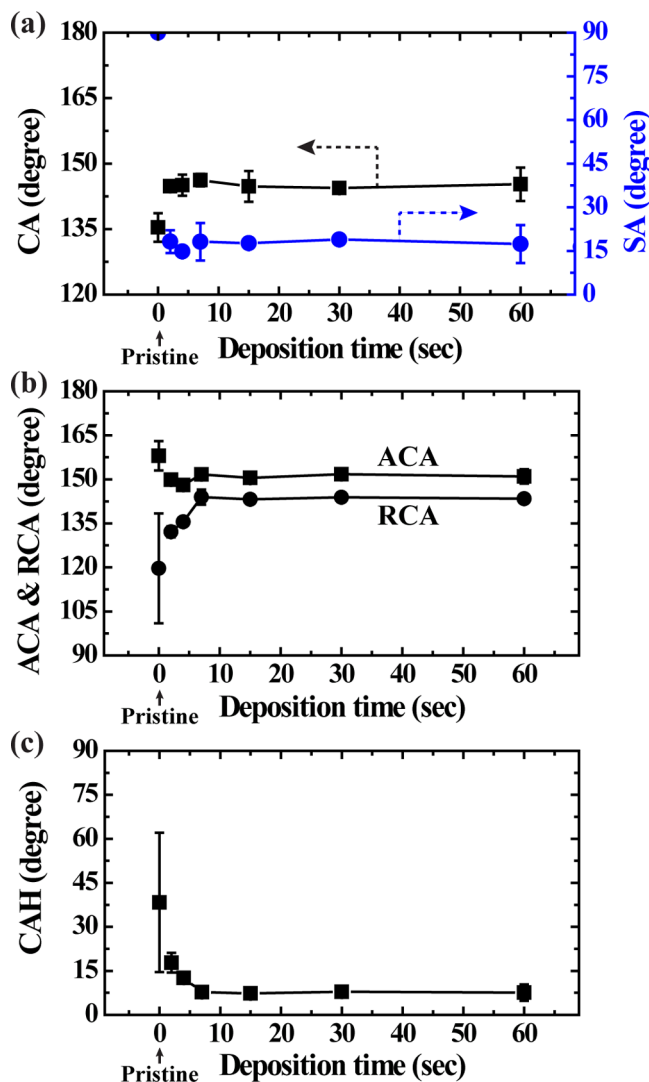
**Figure 2.** Water wettability of GDLs as a function of the HMDSO deposition time and the (a) CA and SA, (b) ACA and RCA, and (c) CAH.

It is clear that the increase in thickness is almost linear at 1.85 nm/sec as the plasma deposition time increased, indicating that the nanolayer thickness can be controlled linearly.

**B. Water Wettability.** Wettability was estimated with respect to the deposition time of the hydrophobic nanolayer. Figure 2 shows the water wettability of the GDLs as a function of the HMDSO deposition time. On the basis of the intrinsic microscale roughness of the microfiber for the GDL, the water CA of the pristine GDL was measured to be 135.4°. After the hydrophobic nanolayer deposition for 2 s on one side of the GDL (GDL-H2s), the CA increased to ~145° and then was saturated regardless of the deposition time. The SA significantly decreased from >90° to <20° after 2 s of deposition time. In particular, the RCAs of the hydrophobic nanolayer GDLs became much higher than those of the pristine GDL as shown in Figure 2b, indicating that the hydrophobic nanolayer could render the GDL surface as self-repellent or slippery.[32] On the basis of the low adhesion between a water droplet and the hydrophobic nanolayer GDL, the CAH measured to be <17.7°, down from 38.3° for the pristine GDL as shown in Figure 2c.

The enhancement of hydrophobicity after nanolayer deposition on porous carbon fiber networks in GDLs is explained with the Cassie−Baxter wetting regime, which describes wetting behavior on a heterogeneous surface consisting of solid and air as[33]

$$\cos \theta^* = rf \cos \theta + f - 1 \qquad (1)$$

where $\theta^*$ is the apparent CA, $r$ is the roughness ratio of the true area of the solid surface to its nominal area, $f$ is the fraction of the projected area of the solid surface that is wet by the liquid, and $\theta$ is the intrinsic CA of the surface material. According to eq 1, lowering the solid fraction and/or increasing the intrinsic CA can lead to an increase in the apparent CA. Because the solid fraction of the GDLs is not affected by the deposition of plasma-polymerized HMDSO (see Figure 1), the observed increase in apparent CA of the hydrophobic nanolayer GDLs may be mainly attributed to an increase in intrinsic CA from approximately 70° to 93° by HMDSO deposition, as reported in refs 30 and 34. As the thickness of the hydrophobic nanolayer increased, the CA and CAH of the GDL are maintained as shown in Figure 2. It is noted that because the deposited nanolayer may uniformly cover the surface after 7 s (16.6 nm) of deposition time, the wettability of the GDL with a hydrophobic nanolayer is substantially unaffected by the layer thickness.

**C. Water Vapor Condensation Behavior.** Water condensation behavior on GDLs was investigated by ESEM
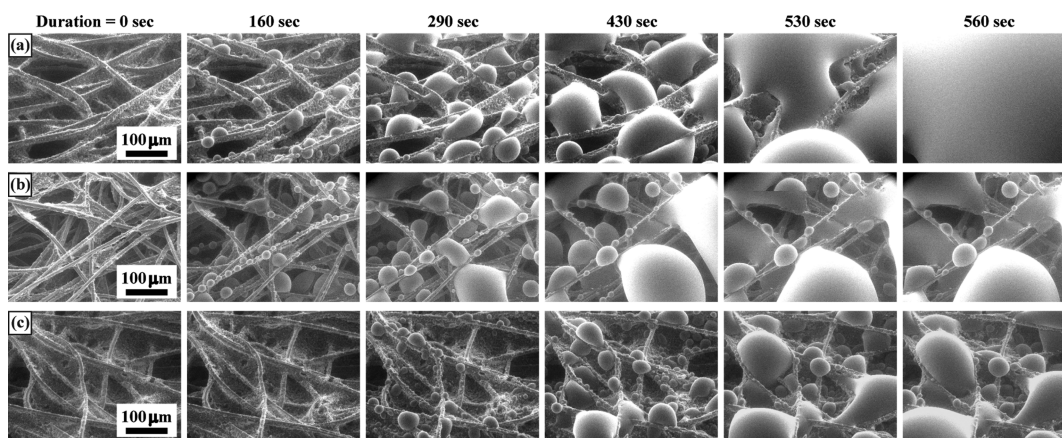


**Figure 3.** A series of ESEM images for water condensation behavior with respect to pressure holding duration for (a) GDL-H0s (pristine GDL), (b) GDL-H4s, and (c) GDL-H30s.
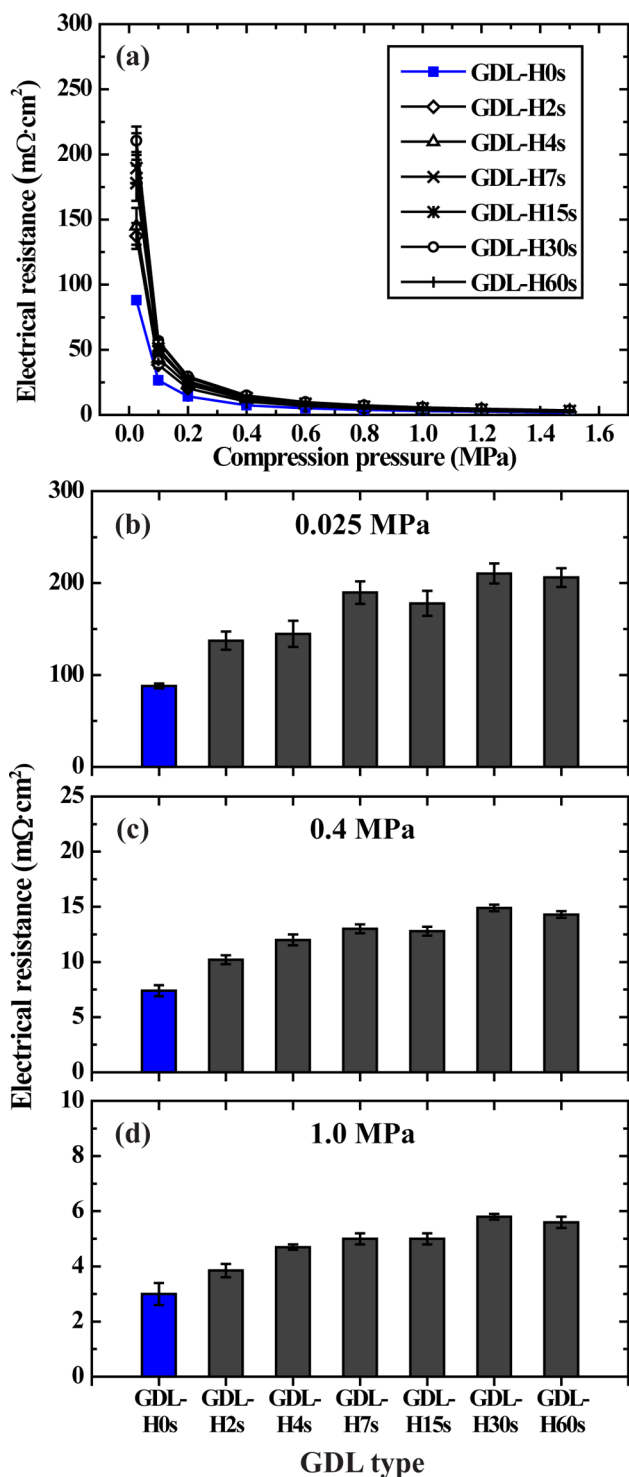
**Figure 4.** (a) Electrical resistances of GDL samples as a function of compression pressure and electrical resistances of GDL samples at specific compression pressures of (b) 0.025, (c) 0.4, and (d) 1.0 MPa.

as shown in Figure 3. As the vapor pressure increases from 3.0 to 5.8 Torr, condensed water is widely distributed on the pristine GDL and blocks the pores between the carbon fibers, which are key paths to mass transport, ultimately causing drastic water flooding. In the cases of the hydrophobic nanolayer GDLs with 8.6 nm (GDL-H4s) and 56.1 nm (GDL-H30s) thicknesses, however, condensed water on the GDLs is observed to cover a much smaller area than that on the
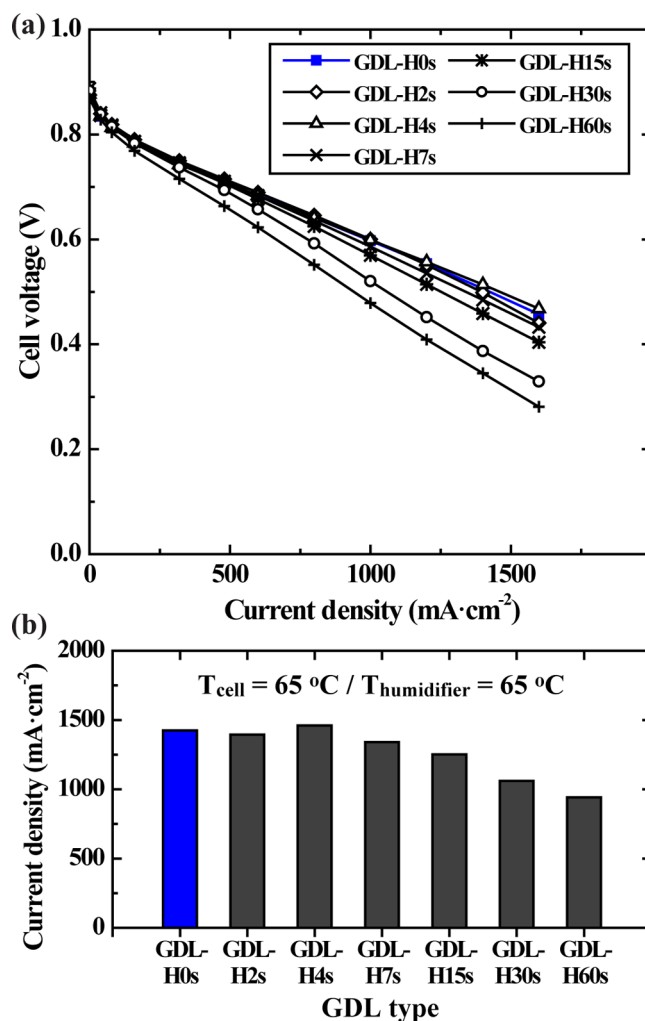


**Figure 5.** Electrochemical performances of fuel cells under normal conditions at 65 °C and RH of 100%/100% for (a) cell voltage as a function of current density and (b) current density at 0.50 V.

pristine GDL. This result is attained due to the low intrinsic surface energy of the silicone-based nanolayers explored in this study. Also, the water condensation rate tends to be suppressed on hydrophobic nanolayer GDLs due to the low surface energy.[29,35] Significant condensation is first observed at 160 s of condensation time on the pristine GDL, whereas the condensation on the hydrophobic nanolayer GDL is mostly suppressed up to 290 s. This suppression of condensation rate is explained through classical nucleation theory, which is related to the free energy barrier for the nucleation of the water nucleus and the intrinsic CA of the surface.[35,36]

$$\Delta G = \pi \gamma r^{*2}(2 - 3\cos\theta + \cos^3\theta)/3 \qquad (2)$$

where $\Delta G$ is free energy barrier for nucleation, $\gamma$ the liquid–vapor surface energy per unit area, $r^*$ the critical radius of formation nucleus, and $\theta$ the intrinsic CA. It is noted that the free energy barrier for nucleation increases when the intrinsic CA increases. The intrinsic wettability of the surface influences the nucleation rate of the droplet, which is expressed in eq 3.

$$J = J_0 \exp(-\Delta G/kT)$$
$$= J_0 \exp\left[-\frac{\pi \gamma r^{*2}(2 - 3\cos\theta + \cos^3\theta)}{3kT}\right] \qquad (3)$$
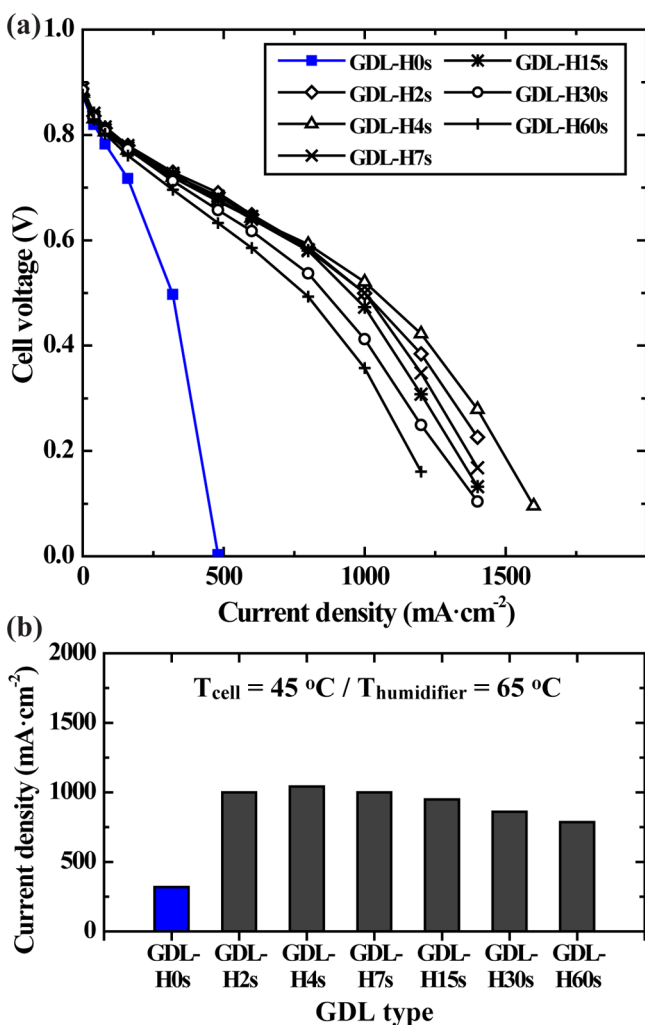
**Figure 6.** Electrochemical performances of fuel cells under a supersaturated condition at 45 °C for (a) cell voltage as a function of current density and (b) current density at 0.50 V.



**Figure 7.** Cell voltages at constant current densities (0, 320, and 1000 mA cm$^{-2}$) under a supersaturated condition at 45 °C for (a) GDL-H0s, (b) GDL-H4s, and (c) GDL-H60s.

where $J$ is the nucleation rate, $J_0$ is a kinetic constant, $k$ is the Boltzmann constant, and $T$ is the absolute temperature. Equation 3 indicates that the nucleation rate of a water droplet could decrease as the intrinsic CA increases. Typically, it is reported that the intrinsic CA of a carbon fiber ranges from 65° to 75°,[37,38] whereas after hydrophobic nanolayer formation, the intrinsic CA is increased to 93° due to the wetting nature of the plasma polymerization of HMDSO.[30] Thus, in considering eq 3, the suppression of water condensation in hydrophobic nanolayer GDLs under supersaturated conditions may result from the high energy barrier for nucleation of the water droplets, which helps to prevent the GDLs from acquiring condensation and subsequent flooding.

**D. Electrical Resistance of GDLs.** Figure 4a shows the electrical resistances of GDL samples as a function of compression pressure. As expected, the electrical resistances of all of the GDLs decreased drastically upon increasing the compression pressure to 0.4 MPa followed by a gradual decrease or static level at compression pressures up to 1.5 MPa, which is attributed to the decrease in contact resistance between carbon fibers in the GDLs by enhancing intimate contact and closing pores as the compression pressure increases. The overall trend of electrical resistance with compression pressure is in good agreement with that reported
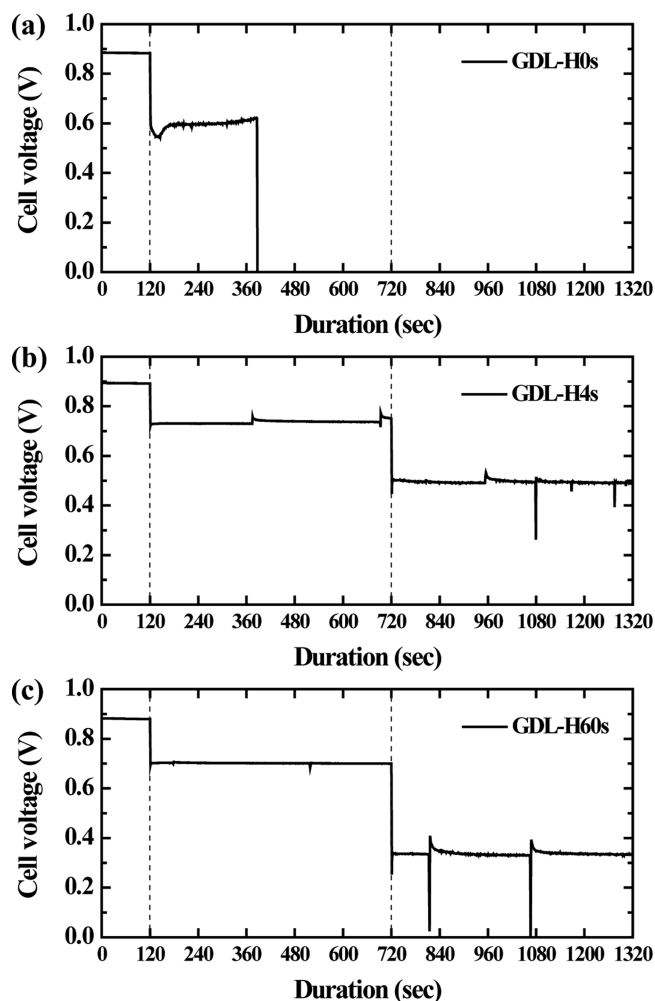
in the literature.[22] Figure 4b−d shows electrical resistances of GDL samples at representative compression pressures of 0.025, 0.4, and 1.0 MPa. It is observed that the pristine GDL (GDL-H0s) exhibits the lowest electrical resistance among all of the GDL samples because it does not contain any hydrophobic agents. The electrical resistances of the HMDSO nanolayer GDLs appear to increase gradually upon increasing the HMDSO deposition time.

**E. Electrochemical $I$−$V$ Performances.** Figure 5 shows the electrochemical performances of fuel cells under normal operating conditions at a $T_{cell}$ of 65 °C and a $T_{humidifier}$ of 65 °C that has an RH of 100%/100%. As shown in Figure 5a, the electrochemical cell performance of the GDL with a hydrophobic nanolayer deposition time of 4 s (GDL-H4s) is essentially the same as or slightly higher than that of the pristine GDL (GDL-H0s) at all current densities. As the hydrophobic nanolayer deposition time increases further from 7 s (GDL-H7s) to 60 s (GDL-H60s), however, the $I$−$V$ performances gradually decrease, as shown in Figure 5a and b. It is thought that even though the hydrophobicity (i.e., CA and CAH) of the GDLs with a hydrophobic nanolayer is much better than that of pristine GDL, the accompanying increase in electrical resistance of the modified GDLs may counterbalance or overwhelm the favorable effect of enhanced hydrophobicity

above a critical nanolayer thickness, especially under relatively mild operating conditions.

To closely examine the cell performance under a severe flooding condition, the electrochemical performances of fuel cells under a supersaturated condition at a $T_{cell}$ of 45 °C and a $T_{humidifier}$ of 65 °C are evaluated as shown in Figure 6. Figure 6a and b clearly demonstrate that the cell performances increase drastically as the hydrophobic nanolayer deposition time increases up to 4 s (GDL-H4s) and then decreases gradually as the hydrophobic nanolayer deposition time further increases from 7 s (GDL-H7s) to 60 s (GDL-H60s). Of interest is that the cell performances of all of the GDLs with hydrophobic nanolayers are much higher than that of the pristine GDL (GDL-H0s). It is thought that under severe water flooding conditions, which typically occur during a cold start-up of FCVs, in contrast to the normal operating conditions, the beneficial effect of enhanced hydrophobicity should be much more important than the detrimental effect of increased electrical resistance, leading to an increase in overall cell performance even for GDL-H60s. Thus, the optimized GDL with a hydrophobic nanolayer thickness of 8.6 nm (GDL-H4s) by the highly efficient "dry" process can impart stable operation to fuel cells under a variety of conditions.

In summary, when the surface of the pristine GDL is modified by HMDSO deposition, the hydrophobic properties (i.e., contact angles, hysteresis, and water condensation behavior) of the GDL are improved dramatically (see Figures 1, 2, and 3). This leads to increased cell performance due to reduced water flooding and enhanced mass transport in fuel cells, but the electrical resistances of the GDL are also increased (see Figure 4), causing decreased cell performance due to increased ohmic resistance in the fuel cells. Thus, the two conflicting properties of the GDL compete with each other as the GDL is modified by HMDSO. Particularly under severe flooding conditions, it appears that the cell performances are increased as the HMDSO deposition time increases up to 4 s (GDL-H4s) due to their enhanced hydrophobic performances, but the cell performances start to decrease as the HMDSO deposition time exceeds 4 s presumably due to an excessive increase in the electrical resistance. Therefore, under the given specific cell configuration and operating conditions of this study, GDL-H4s appears to be optimized to maximize cell performance.

With the aim of evaluating the long-term stability of the fuel cell under supersaturated conditions and the dynamic response to a transient change in FCV speed, the cell voltages upon a rapid change in current density were monitored as shown in Figure 7. Three GDLs (i.e., GDL-H0s, GDL-H4s, and GDL-H60s) were chosen as representative samples. As shown in Figure 7a, the cell voltages of the pristine GDL appear very unstable and suddenly experience catastrophic cell failure even at a low current density of 320 mA cm$^{-2}$ due to severe water flooding. In contrast, the cell voltages of GDL-H4s with a hydrophobic nanolayer thickness of 8.6 nm are likely to be stable even at a high current density of 1000 mA cm$^{-2}$ for 10 min due to its enhanced hydrophobicity. Surprisingly, even GDL-H60s can be operated at 1000 mA cm$^{-2}$ for 10 min. Thus, it is thought that GDL-H4s performs much better than the pristine GDL (GDL-H0s) in terms of operational stability and dynamic response under a severe water flooding condition.

## 4. CONCLUSION

Silicone-based hydrophobic nanolayers at controlled thicknesses were deposited on GDLs using PECVD. Water wettability on the hydrophobic nanolayer GDLs was explored by considering macroscale droplet repellency and microscale condensation suppression. After hydrophobic nanolayer deposition on the GDL surfaces, the CA increases from 135.4° (pristine) to ~145°. SA significantly decreases from >90° (pristine) to <20°, becoming slippery surfaces of which water droplets easily roll off. Water condensation was also suppressed on the GDLs with the hydrophobic nanolayer due to the easy roll off nature with the high CA and low CAH. Electrical resistances of GDLs with a hydrophobic nanolayer increased with HMDSO deposition time or nanolayer thickness. Under normal conditions, the electrochemical performance of the GDL with a hydrophobic nanolayer thickness of 8.6 nm (GDL-H4s) was virtually the same as that of the pristine GDL. Under a supersaturated condition, however, GDL-H4s exhibited a much better cell performance than that of the pristine GDL due to enhanced hydrophobicity. The long-term operational stability and dynamic response of GDL-H4s were much better than those of the pristine GDL. Thus, the hydrophobic nanolayer deposition process based on silicone materials is a highly efficient and cost-effective "dry" process for GDL, which can impart enhanced operational stability on PEMFCs, especially under severe flooding conditions. This novel "dry" process for GDLs is a prospective substitute for the conventional "wet" dip-coating process using expensive PTFE and solvents over long treatment times.

## ■ AUTHOR INFORMATION

### Corresponding Authors
*E-mail: boki.hong@hyundai.com. Tel: +82 31 899 3202. Fax: +82 31 368 3331. Address: 104 Mabuk-Dong, Giheung-Gu, Yongin-Si, Gyeonggi-Do 446-912, Republic of Korea.
*E-mail: mwmoon@kist.re.kr. Tel: +82 2 958 5487. Fax: +82 2 958 5509. Address: Hwarangno 14-gil 5, Seongbuk-gu, Seoul 136-791, Republic of Korea.

### Notes
The authors declare no competing financial interest.

## ■ REFERENCES

(1) Gamburzev, S.; Appleby, A. J. Recent Progress in Performance Improvement of the Proton Exchange Membrane Fuel Cell (PEMFC). *J. Power Sources* **2002**, *107*, 5−12.

(2) Han, K.; Hong, B. K.; Kim, S. H.; Ahn, B. K.; Lim, T. W. Influence of Anisotropic Bending Stiffness of Gas Diffusion Layers on the Electrochemical Performances of Polymer Electrolyte Membrane Fuel Cells. *Int. J. Hydrogen Energy* **2010**, *35*, 12317−12328.

(3) Jiao, K.; Zhou, B. Innovative Gas Diffusion Layers and Their Water Removal Characteristics in PEM Fuel Cell Cathode. *J. Power Sources* **2007**, *169*, 296−314.

(4) Li, H.; Tang, Y. H.; Wang, Z. W.; Shi, Z.; Wu, S. H.; Song, D. T.; Zhang, J. L.; Fatih, K.; Zhang, J. J.; Wang, H. J.; Liu, Z. S.; Abouatallah, R.; Mazza, A. A Review of Water Flooding Issues in the Proton Exchange Membrane Fuel Cell. *J. Power Sources* **2008**, *178*, 103−117.

(5) Farooque, M.; Maru, H. C. Fuel Cells - The Clean and Efficient Power Generators. *Proc. IEEE* **2001**, *89*, 1819−1829.

(6) Baschuk, J.; Li, X. Modelling of Polymer Electrolyte Membrane Fuel Cells with Variable Degrees of Water Flooding. *J. Power Sources* **2000**, *86*, 181−196.

(7) Shimpalee, S.; Beuscher, U.; Van Zee, J. W. Analysis of GDL Flooding Effects on PEMFC Performance. *Electrochim. Acta* **2007**, *52*, 6748−6754.

(8) Su, A.; Weng, F. B.; Hsu, C. Y.; Chen, Y. M. Studies on Flooding in PEM Fuel Cell Cathode Channels. *Int. J. Hydrogen Energy* **2006**, *31*, 1031−1039.

(9) Neyerlin, K.; Gasteiger, H. A.; Mittelsteadt, C. K.; Jorne, J.; Gu, W. Effect of Relative Humidity on Oxygen Reduction Kinetics in a PEMFC. *J. Electrochem. Soc.* **2005**, *152*, A1073−A1080.

(10) Xu, H.; Song, Y.; Kunz, H. R.; Fenton, J. M. Effect of Elevated Temperature and Reduced Relative Humidity on ORR Kinetics for PEM Fuel Cells. *J. Electrochem. Soc.* **2005**, *152*, A1828−A1836.

(11) Bi, W.; Fuller, T. F. Temperature Effects on PEM Fuel Cells Pt/ C Catalyst Degradation. *J. Electrochem. Soc.* **2008**, *155*, B215−B221.

(12) Pasaogullari, U.; Wang, C. Y. Liquid Water Transport in Gas Diffusion Layer of Polymer Electrolyte Fuel Cells. *J. Electrochem. Soc.* **2004**, *151*, A399−A406.

(13) Mathias, M. F.; Roth, J.; Fleming, J.; Lehnert, W. Diffusion Media Materials and Characterisation. In *Handbook of Fuel Cells*; Vielstich, W., Gasteiger, H. A., Lamm, A., Eds.; John Wiley & Sons, Ltd.: New York, 2003; pp 517−537.

(14) Saleh, M. M.; Okajima, T.; Hayase, M.; Kitamura, F.; Ohsaka, T. Exploring the Effects of Symmetrical and Asymmetrical Relative Humidity on the Performance of $H_2$/Air PEM Fuel Cell at Different Temperatures. *J. Power Sources* **2007**, *164*, 503−509.

(15) Escribano, S.; Blachot, J.-F.; Ethève, J.; Morin, A.; Mosdale, R. Characterization of PEMFCs Gas Diffusion Layers Properties. *J. Power Sources* **2006**, *156*, 8−13.

(16) Lim, C.; Wang, C. Y. Effects of Hydrophobic Polymer Content in GDL on Power Performance of a PEM Fuel Cell. *Electrochim. Acta* **2004**, *49*, 4149−4156.

(17) Park, G. G.; Sohn, Y. J.; Yang, T. H.; Yoon, Y. G.; Lee, W. Y.; Kim, C. S. Effect of PTFE Contents in the Gas Diffusion Media on the Performance of PEMFC. *J. Power Sources* **2004**, *131*, 182−187.

(18) Park, S.; Lee, J. W.; Popov, B. N. Effect of PTFE Content in Microporous Layer on Water Management in PEM Fuel Cells. *J. Power Sources* **2008**, *177*, 457−463.

(19) Velayutham, G.; Kaushik, J.; Rajalakshmi, N.; Dhathathreyan, K. S. Effect of PTFE Content in Gas Diffusion Media and Microlayer on the Performance of PEMFC Tested under Ambient Pressure. *Fuel Cells* **2007**, *7*, 314−318.

(20) Rofaiel, A.; Ellis, J. S.; Challa, P. R.; Bazylak, A. Heterogeneous through-Plane Distributions of Polytetrafluoroethylene in Polymer Electrolyte Membrane Fuel Cell Gas Diffusion Layers. *J. Power Sources* **2012**, *201*, 219−225.

(21) Wang, Y.; Al Shakhshir, S.; Li, X. Fabrication of Hydrophobic Coating on GDL with Silicone Based Materials. *ECS Trans.* **2010**, *28*, 301−306.

(22) Ismail, M. S.; Damjanovic, T.; Ingham, D. B.; Pourkashanian, M.; Westwood, A. Effect of Polytetrafluoroethylene-Treatment and Microporous Layer-Coating on the Electrical Conductivity of Gas Diffusion Layers Used in Proton Exchange Membrane Fuel Cells. *J. Power Sources* **2010**, *195*, 2700−2708.

(23) Améduri, B.; Boutevin, B.; Kostov, G. Fluoroelastomers: Synthesis, Properties and Applications. *Prog. Polym. Sci.* **2001**, *26*, 105−187.

(24) Pai, Y.-H.; Ke, J.-H.; Huang, H.-F.; Lee, C.-M.; Zen, J.-M.; Shieu, F.-S. $CF_4$ Plasma Treatment for Preparing Gas Diffusion Layers in Membrane Electrode Assemblies. *J. Power Sources* **2006**, *161*, 275−281.

(25) Lee, C.-M.; Pai, Y.-H.; Zen, J.-M.; Shieu, F.-S. Characterization of Teflon-Like Carbon Cloth Prepared by Plasma Surface Modification for Use as Gas Diffusion Backing in Membrane Electrode Assembly. *Mater. Chem. Phys.* **2009**, *114*, 151−155.

(26) Lee, C.-M.; Pai, Y.-H.; Lin, G.-R.; Shieu, F.-S. Teflon-Coated Carbon Fiber Core/Shell Structure Based Hydrophobic Gas-Diffusion Electrode for Proton Exchange Membrane Fuel Cells. *J. Electrochem. Soc.* **2010**, *157*, B256−B259.

(27) Siliprandi, R.; Zanini, S.; Grimoldi, E.; Fumagalli, F.; Barni, R.; Riccardi, C. Atmospheric Pressure Plasma Discharge for Polysiloxane Thin Films Deposition and Comparison with Low Pressure Process. *Plasma Chem. Plasma Process.* **2011**, *31*, 353−372.

(28) Her, E. K.; Ko, T.-J.; Lee, K.-R.; Oh, K. H.; Moon, M.-W. Bioinspired Steel Surfaces with Extreme Wettability Contrast. *Nanoscale* **2012**, *4*, 2900−2905.

(29) Ko, T.-J.; Her, E. K.; Shin, B.; Kim, H.-Y.; Lee, K.-R.; Hong, B. K.; Kim, S. H.; Oh, K. H.; Moon, M.-W. Water Condensation Behavior on the Surface of a Network of Superhydrophobic Carbon Fibers with High-Aspect-Ratio Nanostructures. *Carbon* **2012**, *50*, 5085−5092.

(30) Rahmawan, Y.; Moon, M.-W.; Kim, K.-S.; Lee, K.-R.; Suh, K.-Y. Wrinkled, Dual-Scale Structures of Diamond-Like Carbon (DLC) for Superhydrophobicity. *Langmuir* **2010**, *26*, 484−491.

(31) Park, G.-G.; Park, J.-S.; Kim, M.-J.; Sohn, Y.-J.; Park, S.-H.; Yim, S.-D.; Yang, T.-H.; Yoon, Y.-G.; Lee, W.-Y.; Kim, C.-S. Integrated Multi-Measurement System for Measuring Physical Properties of Gas Diffusion Layer for Polymer Electrolyte Fuel Cell with Respect to Compression. U.S. Patent 20100236335, September 23, 2010.

(32) Briscoe, B. J.; Williams, D. R.; Galvin, K. P. Condensation on Hydrosol Modified Polyethylene. *Colloids Surf., A* **2005**, *264*, 101−105.

(33) Marmur, A. Wetting on Hydrophobic Rough Surfaces: To Be Heterogeneous or Not to Be? *Langmuir* **2003**, *19*, 8343−8348.

(34) Parry, V.; Berthomé, G.; Joud, J.-C. Wetting Properties of Gas Diffusion Layers: Application of the Cassie−Baxter and Wenzel Equations. *Appl. Surf. Sci.* **2012**, *258*, 5619−5627.

(35) Varanasi, K. K.; Hsu, M.; Bhate, N.; Yang, W. S.; Deng, T. Spatial Control in the Heterogeneous Nucleation of Water. *Appl. Phys. Lett.* **2009**, *95*, 094101-1−094101-3.

(36) Lee, A.; Moon, M.-W.; Lim, H.; Kim, W.-D.; Kim, H.-Y. Water Harvest Via Dewing. *Langmuir* **2012**, *28*, 10183−10191.

(37) Bismarck, A.; Kumru, M. E.; Springer, J. Influence of Oxygen Plasma Treatment of PAN-Based Carbon Fibers on Their Electrokinetic and Wetting Properties. *J. Colloid Interface Sci.* **1999**, *210*, 60−72.

(38) Song, W.; Gu, A.; Liang, G.; Yuan, L. Effect of the Surface Roughness on Interfacial Properties of Carbon Fibers Reinforced Epoxy Resin Composites. *Appl. Surf. Sci.* **2011**, *257*, 4069−4074.